Monday, October 19, 2026

Manuscript ID: egusphere-2026-3702

Manuscript title: “Single-Particle Polarization Tomography Enables Highly Accurate Phase Identification of Cloud Particles”

Authors: Yang Chen, Xiang Xu, Ruishan Xiao, Fangzhen Yao, Xiaojing Shi, Jiaxin Wang, Jun Wang, Gu Liang, and Zhiguo Yue

Dear Referee,

We would like to sincerely thank you for your constructive comments on our manuscript submitted to Atmospheric Measurement Techniques. We have carefully considered all of your comments and suggestions. These comments are very helpful for improving the clarity and quality of our manuscript. Since the manuscript is currently in the public discussion stage, we provide our detailed point-by-point responses below and indicate the corresponding revisions that have been made in the revised manuscript.

The detailed responses are provided below:

~~~~~~
~~~~~~

Reviewers' comments:

From Reviewer 2

Reviewer #2: Review of 'Single-Particle Polarization Tomography Enables Highly Accurate Phase Identification of Cloud Particles' by Yang Chen et al.

The manuscript introduces a polarization tomographic imaging method to identify the phase of cloud chamber generated clouds. The method combines digital holography with polarimetric imaging. For cloud particles with sizes below 50 µm the cloud particle circularity and degree of linear polarization are used for phase identification. A linear support vector machine is used to distinguish liquid from frozen particles based on the two parameters. As an example of the methods a 10 s time window of a glaciation evolution of a cloud chamber generated mixed-phase cloud is presented where the microphysical properties of the cloud particles are derived with the tomographic imaging method.

While I request a few adaptations to the manuscript (see comments below), the method seems promising for the characterization of mixed-phase clouds and is in the scope of AMT. Therefore, I recommend the manuscript to be published after major revisions.

General comments:

Comment #1: Please elaborate what the reference is for validating liquid and frozen particles. Maybe I missed this in the manuscript. But how did

you know the real phase of the particles where the calculation of accuracy, precision, recall, etc. is based on.

Reply #1:

We thank the reviewer for this question. We established a reference dataset comprising 200 liquid droplets and 200 ice crystals based on the experimental stages and identifiable morphological features in reconstructed images. After the atomizer began supplying fog and before AgI introduction, the chamber predominantly contained supercooled liquid droplets. Particles collected during this stage were used as liquid-droplet reference samples. After AgI introduction, the chamber entered a mixed-phase state in which liquid droplets and ice crystals coexisted. We selected particles exhibiting clear crystalline morphological features in the reconstructed images as ice-crystal reference samples, as shown in Fig. R1. We did not label all particles collected during this stage as ice crystals. Accuracy, precision, and recall quantify agreement between the classification results and these reference labels.

During the actual glaciation process, many particles cannot be reliably distinguished as liquid droplets or ice crystals based on morphology alone. This illustrates the limitations of morphology-based phase identification and further highlights the need to incorporate polarization information to assist phase discrimination. For subsequent continuous-process analyses, including LWC and particle number concentration, we use particles

detected throughout the observation period. Their phases are assigned using the developed dual-parameter method. We will add the reference-sample selection and labeling procedures to the Methods section and clarify which samples are used to evaluate classification performance.

The corresponding text has been revised as follows: *"To construct a reference dataset with reliable phase labels, liquid-droplet samples were selected from the period before silver iodide (AgI) introduction, when the chamber predominantly contained supercooled liquid droplets. After AgI introduction, the chamber entered a mixed-phase state in which liquid droplets and ice crystals coexisted. Therefore, ice-crystal samples used for the reference dataset were selected only from particles whose reconstructed images exhibited clear crystalline morphological features that allowed reliable phase determination. This screening criterion was applied only to ensure reliable phase labels for the reference samples used for model training and evaluation. However, during the actual mixed-phase glaciation process, many particles could not be reliably distinguished as liquid droplets or ice crystals based on morphology alone."* This revision has been added in **Sect. 2.3, p. 8. in the revised manuscript.** The applicable conditions are described as follows: *"Reference labels were established from experimental stages and clear crystalline morphology. Although this supports label reliability, the reference dataset has limited representativeness for morphologically ambiguous or nearly spherical ice*

crystals. The classification metrics therefore describe performance for the current reference samples; applicability to additional particle types and independent experimental conditions requires further validation." This revision has been added in **Sect. 5, p. 22. in the revised manuscript.**

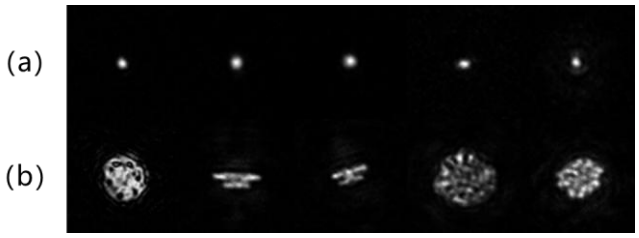

Figure R1. Representative reconstructed images of reference particles. (a) Liquid droplets; (b) ice crystals.

Comment #2: The discussion chapter contains the description of the machine learning linear support vector machine as well as the results. While accuracy, precision, recall should be discussed in the discussion section, I recommend to move the machine learning method in the methods section and the results in the results section.

Reply #2:

We thank the reviewer for the suggestion. We agree that the original Discussion combined the classification method, results, and interpretation. The revised manuscript now presents reference-sample selection, the linear SVM formulation, input features, class labels, the training/test split, the

decision rule, and definitions of accuracy, precision, and recall in the new Sect. 2.3, 'Phase classification method', including Eqs. (21)–(27).

The classification results, decision boundary, confusion matrices, and performance comparison are presented in Sect. 4.2, Fig. 9, and Table 2. The continuous cloud-chamber observations are presented separately in Sect. 4.3 and Fig. 10. Section 5 discusses feature complementarity, possible causes of misclassification, the reference-label selection, and the conditions under which the results apply. This structure separates the method and observed results from their interpretation.

Comment #3: Furthermore, the results of the glaciation experiment in the cloud chamber are also presented in the discussion section. Why are they not in the results section? The discussion section should be about the interpretation of the results not presenting additional results.

Reply #3:

We thank the reviewer for pointing out the section-placement issue. The cloud-chamber time series have been moved from the Discussion to the new Sect. 4.3, 'Continuous observations of cloud chamber dynamics'. Figure 10 and its accompanying results describe liquid water content, liquid droplet and ice crystal number concentrations, number fractions, and mean equivalent diameter during the selected 10 s window.

Section 5 now contains the interpretation of these observations, including the effects of phase assignment on LWC and the conditional interpretation of the changes in phase composition and mean diameter. The interpretation refers to inferred LWC and limits the evidence for reduced classification errors to the reference-sample test set.

Comment #4: Please discuss the measurement uncertainty for the particle size. You performed measurements with glass beads, but no final conclusion is taken here.

Reply #4:

We thank the reviewer for this comment. We have expanded the particle-sizing evaluation in Sect. 4.1 to distinguish deviations of group-mean diameter from the size variability of the reference particles. The measurements used Thermo Fisher Scientific 9000 Series glass microspheres with reference mean diameters of 5.1, 10.0, and 49.0 µm. Because the true diameter of each individual microsphere was not independently established, the measured group means were compared with the manufacturer-supplied reference means. The results are shown in Table R1.

The measured mean diameters were 5.12, 10.39, and 50.69 µm, with measured diameter-distribution SDs of 0.48, 0.88, and 1.42 µm. Relative deviations calculated from the unrounded measured means were +0.41%,

+3.92%, and +3.45%, respectively. The manufacturer-supplied diameter-distribution SDs were 0.6, 1.1, and 2.4 μm. Thus, the measured distribution SD contains both intrinsic particle-size variation and measurement effects and cannot be used directly as the measurement uncertainty of a single particle.

We have replaced the original inference based on whether individual measurements fell within the manufacturer's diameter ranges with this quantitative comparison of means. We have also added a discussion of object-space pixel scaling, reconstruction-plane selection, image noise, and segmentation. Thresholding, morphological processing, and hole filling can change projected area and equivalent diameter, with a potentially larger relative effect on small particles. The existing measurements quantify reference-mean deviations but do not separately resolve all contributions to a full particle-size uncertainty budget.

The corresponding text has been revised as follows: *"To evaluate particle sizing performance, validation measurements were conducted using Thermo Fisher Scientific 9000 Series glass microsphere standards. The three groups had reference diameters of 5.1 ± 0.5, 10.0 ± 1.0, and 49.0 ± 1.4 μm. Figure 4a–c shows the results. Because the true diameter of each microsphere was not independently established, performance was evaluated by comparing measured and reference mean diameters. Table 1 summarizes the measurements. Relative deviations of the measured means*

were approximately 0.4%–3.9%, calculated from the unrounded measured means. These comparisons provide a quantitative assessment of sizing performance under the tested conditions." This clarification has been added in **Sect. 4.1, p. 13. in the revised manuscript.**

"The reference standard deviations of the microsphere diameter distributions show that the standards themselves vary in size. The measured diameter SD therefore includes both the intrinsic size distribution and measurement effects, and cannot directly represent the measurement uncertainty of an individual microsphere diameter. Finite sampling may also affect the comparison between measured and reference means." This clarification has been added in **Sect. 4.1, p. 14. in the revised manuscript.**

"Particle sizing is influenced by object-space pixel scaling, reconstruction-plane selection, image noise, and particle boundary segmentation. Thresholding, morphological processing, and hole filling can alter projected area and hence equivalent diameter. For small particles, the same boundary displacement can produce a larger relative diameter error. The microsphere experiments quantify deviations of measured means from reference means. However, the available data do not separately quantify all contributions and therefore do not establish the full particle diameter measurement uncertainty." This clarification has been added in **Sect. 4.1, p. 14. in the revised manuscript.**

Table R1: Comparison of reference diameter parameters and measurements for three groups of standard glass microspheres.

Reference mean diameter (µm)	Measured mean diameter (µm)	Reference diameter distribution SD (µm)	Measured diameter distribution SD (µm)	Relative deviation of mean (%)
5.1	5.12	0.6	0.48	+0.41
10.0	10.39	1.1	0.88	+3.92
49.0	50.69	2.4	1.42	+3.45

Comment #5: Introduction: There are studies on in-situ single particle phase discrimination based on the light scattering properties e.g. Waitz et al. (2021), Kaye et al. (2008) or Ulanowski et al. (2014). Please also refer to these.

Reply #5:

We thank the reviewer for recommending these relevant studies. We have expanded the in situ measurement background in the Introduction to include Kaye et al. (2008), Ulanowski et al. (2014), and Waitz et al. (2021), and have added their complete entries to the reference list.

The revised paragraph distinguishes direct particle imaging from measurements based on single-particle light scattering. It identifies spatial scattering patterns as a source of morphological information, scattering-pattern texture as a measure of ice crystal roughness or complexity, and angular-scattering functions as a basis for phase identification. The corresponding text has been revised as follows: *"Single-particle light scattering also provides morphological and phase information. Examples include spatial scattering patterns for morphological analysis (Kaye et al.,*

2008), scattering-pattern texture for ice crystal roughness and structural complexity (Ulanowski et al., 2014), and angular-scattering functions for phase identification (Waitz et al., 2021).” This clarification has been added in **Sect. 1, p. 2. in the revised manuscript.**

Comment #6: Please provide more information on the cloud chamber characteristics: Volume, cleaning procedures before experiments, experiments preparation, how is the supersaturation controlled? Which instruments are used to monitor temperature, humidity, aerosol population?

Reply #6:

We thank the reviewer for requesting further experimental details. We have expanded Sect. 3 to describe the chamber volume, preparation and cleaning procedures, environmental monitoring, and the observation of cloud particles. The chamber volume was 0.213 m^3. Between experiments, fog was supplied continuously for several minutes to clean the chamber and reduce residual particles. For each experiment, the chamber was cooled to −25 °C, the built-in atomizer was activated to establish a supercooled-droplet environment, and AgI smoke generated by burning the seeding agent was introduced through a tube. The polarization tomographic imaging instrument observed liquid droplets and ice crystals in situ in the upper observation region.

Supersaturation was not directly controlled. Instead, the supply of water droplets was varied by adjusting the fog-supply duration, and the revised text now states this operating procedure explicitly. Chamber temperature, humidity, and pressure were monitored using electronic temperature, humidity, and pressure sensors and a PT100 temperature probe, with the readings displayed by the control system.

We have also distinguished the monitored particle populations. The polarization tomographic imaging system retrieved cloud-particle diameter, morphology, polarization parameters, and number concentration. The existing transmission microscopy system observed ice crystals that had grown and settled onto a sampling window. When dense ice coverage prevented individual crystals from being resolved, the window was manually cleaned with anhydrous ethanol. The number concentration and size distribution of AgI aerosol particles that had not nucleated ice were not measured directly. The corresponding text has been revised as follows:

"Liquid droplet and ice crystal observations were conducted in an ice cloud chamber with a volume of 0.213 m³. Figure 2 shows the experimental configuration and procedure. The polarization tomographic imaging instrument was installed in the upper observation region for in situ measurements. Between experiments, fog was supplied continuously for several minutes to clean the chamber and reduce residual particles from the preceding experiment. The chamber was first cooled to −25 °C using a

refrigeration compressor. The built-in atomizer was then activated to supply supercooled droplets and establish a supercooled-droplet environment. Smoke generated by burning an AgI seeding agent was introduced through a tube to promote heterogeneous nucleation and ice crystal formation. The resulting ice crystals could grow through vapor deposition and collisions. The polarization tomographic imaging system measured liquid droplets and ice crystals in situ within the observation region. Supercooled-water supply was varied by adjusting the fog-supply duration; supersaturation was not directly controlled. Electronic temperature, humidity, and pressure sensors and a PT100 temperature probe monitored chamber conditions, which were displayed by the control system in real time. The imaging system retrieved particle diameter, morphology, polarization parameters, and number concentration. The chamber's existing transmission microscopy system mainly observed ice crystals that had grown and settled onto a sampling window under gravity. When dense ice coverage prevented individual crystals from being resolved, the window was manually cleaned with anhydrous ethanol. The number concentration and size distribution of AgI aerosol particles that had not nucleated ice were not measured directly." This clarification has been added in **Sect. 3, pp. 11–12. in the revised manuscript.**

Comment #7: Is there a limitation in maximum particle concentration of the instrument?

Reply #7:

We thank the reviewer for the question. High particle concentrations can limit single-particle measurements because overlapping diffraction signals and an increased out-of-focus background make focusing and segmentation more difficult. Closely spaced particles may also be missed or merged, affecting diameter, morphology, and number-concentration estimates.

Under the current system configuration and processing conditions, the upper end of the particle number concentration range tested in this study was 2000 cm^{-3}. This value describes the tested range, rather than a universal maximum measurable concentration for all particle-size distributions and observation conditions. We have added the explanation of high-concentration effects and made this distinction explicit in Sect. 5. The corresponding text has been revised as follows: *"Under the current system configuration and processing conditions, the upper end of the tested particle number concentration range was 2000 cm^{-3}. This value describes the tested range and does not establish a universal maximum measurable concentration for different size distributions and observation conditions. At higher particle concentrations, overlapping diffraction signals and out-of-focus background can hinder focusing and segmentation. Closely*

spaced particles may be missed or merged, affecting diameter, morphology, and number-concentration estimates." This clarification has been added in **Sect. 5, p. 22. in the revised manuscript.**

Comment #8: Please add missing references for the used definitions. E.g. for accuracy, precision, recall, dolp the references are missing.

Reply #8:

We thank the reviewer for this suggestion. We have added Powers (2011) to the definitions of accuracy, precision, and recall in Sect. 2.3, Eqs. (25)–(27). The revised text explicitly defines ice crystals as the positive class and liquid droplets as the negative class, and defines TP, TN, FP, and FN accordingly. We have also added Li et al. (2023) to the DoLP definitions in Sect. 2.1, Eqs. (8) and (11).

Meanwhile, we reviewed the references in other parameter definitions and added new references to the list of references, making the definitions and calculation bases of each indicator more clear.

Specific comments:

Comment #9: L56-59: please refer to the original literature in distinguishing liquid from ice phase using polarization lidar (e.g. Liou and Lahore, 1974 etc.). This is not a recent finding from 5 years ago.

Reply #9:

We thank the reviewer for this suggestion. We agree that cloud phase identification using polarization lidar has a long history and that the original Introduction did not adequately acknowledge its early foundations. We have added Liou and Lahore (1974) to describe the early theoretical and experimental basis for using backscatter depolarization differences between spherical water droplets and nonspherical ice crystals for cloud phase identification. Recent references have been retained to describe subsequent developments and applications. The corresponding text has been revised as follows: *"Early theoretical and experimental studies established the use of backscatter depolarization differences between spherical water droplets and nonspherical ice crystals for cloud phase identification (Liou and Lahore, 1974)."* This clarification has been added in **Sect. 1, p. 2. in the revised manuscript.**

Comment #10: L89: Please state measurement uncertainty for mean particle sizes here. How is the size of the ice particles calculated? Is it the maximum dimension?

Reply #10:

We thank the reviewer for requesting this clarification. Both liquid-droplet and ice-crystal sizes are reported as projected-area equivalent diameters, defined as the diameter of a circle with the same area as the segmented particle projection. Equation (17) in Sect. 2.2 gives the calculation, where Ap is the particle area in pixels, p = 3.45 μm is the camera pixel size, and G = 5 is the imaging magnification. For ice crystals, this diameter describes the projection in the current viewing direction and is not the maximum particle dimension.

$$D_{eq} = \frac{2}{G}\sqrt{\frac{A_p p^2}{\pi}} \tag{R1}$$

The liquid-droplet and ice-crystal reference groups each contain 200 particles. Their mean equivalent diameters are 4.66 and 25.36 μm, and the corresponding diameter-distribution SDs are 1.05 and 8.72 μm. Under an independent-sampling approximation, $\mathrm{SE} = \mathrm{SD}/\sqrt{n}$ gives sampling standard errors of 0.074 and 0.617 μm for the two means, respectively. These SEs describe conditional sampling variability in the selected reference samples; they do not include common scale-calibration errors or

systematic boundary-extraction effects and therefore are not complete measurement uncertainties of the mean diameters.

We have clarified the size definition in Sect. 2.2 and separately reported the means, distribution SDs, and sampling SEs in Sect. 4.1. The main measurement influences and the limits of the available uncertainty assessment are also explained in Sect. 4.1.

The corresponding text has been revised as follows: *"where Ap is the projected particle area in pixels, p = 3.45 μm is the camera pixel size, and G = 5 is the imaging magnification. Equation (17) gives the diameter of a circle with the same area as the two-dimensional particle projection, namely the projected-area equivalent diameter. This definition is used for both liquid droplets and ice crystals in this study. For ice crystals, the reported diameter corresponds to the projected area in the current viewing direction rather than the maximum particle dimension."* This clarification has been added in **Sect. 2.2, Eq. (17), p. 7. in the revised manuscript.**

"Droplet sizes ranged from 2.7–8.9 μm, with a mean of 4.66 μm (SD = 1.05 μm) and a coefficient of variation of 22.6%." This clarification has been added in **Sect. 4.1, p. 14. in the revised manuscript.**

"Ice crystal sizes ranged from 8.9–53.3 μm, with a mean of 25.36 μm (SD = 8.72 μm) and a coefficient of variation of 34.4%. Here, the diameter distribution SD describes size variability between particles. Under an independent-sampling approximation, $\mathrm{SE} = \mathrm{SD}/\sqrt{n}$ *gives sampling*

standard errors of 0.074 and 0.617 µm for the mean liquid droplet and ice crystal diameters, respectively. Each group contained 200 particles. SE describes sampling variability in the estimated mean and does not replace its full measurement uncertainty." This clarification has been added in **Sect. 4.1, p. 14. in the revised manuscript.**

Comment #11: L95 and L375-L378: What is the reference for the validation? How do you know the real particle phase? Is it before and after the addition of INPs to the cloud chamber? How do you know all particle nucleated? Also 98.33% suggest more robust statistics than 60/61 samples. I would suggest to say 98% instead keeping the number of significant digits. Similar for accuracy, precision, recall.

Reply #11:

We thank the reviewer for these comments. We did not assume that all droplets froze after AgI introduction, nor did we label every particle observed after AgI introduction as ice. Liquid-droplet reference samples were selected from the observations before AgI introduction. Ice-crystal reference samples were selected from the subsequent mixed-phase observations only when the reconstructed images showed clear crystalline morphological features that supported phase assignment. Representative reference particles are shown in Fig. R1. We have clarified this labeling procedure in Sect. 2.3 and explained in Sect. 5 that the resulting

performance metrics apply to this reference dataset, whose representativeness for morphologically ambiguous or nearly spherical ice crystals is limited.

The test set contains 120 particles, comprising 58 liquid droplets and 62 ice crystals. The dual-parameter SVM method correctly classified 57 liquid droplets and 61 ice crystals, with one error in each class. Its overall accuracy is therefore 118/120, approximately 98%. We have adopted the suggested rounding, consistently reporting the overall accuracy as approximately 98% in the Abstract, Introduction, Results, and Conclusions. Accuracy, precision, and recall are reported as percentages rounded to whole numbers, while the integer counts are retained in the confusion matrices.

The corresponding text has been revised as follows: *"To construct a reference dataset with reliable phase labels, liquid-droplet samples were selected from the period before silver iodide (AgI) introduction, when the chamber predominantly contained supercooled liquid droplets. After AgI introduction, the chamber entered a mixed-phase state in which liquid droplets and ice crystals coexisted. Therefore, ice-crystal samples used for the reference dataset were selected only from particles whose reconstructed images exhibited clear crystalline morphological features that allowed reliable phase determination."* This clarification has been added in **Sect. 2.3, p. 8. in the revised manuscript.**

"The test set contained 120 particles, including 58 liquid droplets and 62 ice crystals. The dual-parameter SVM method correctly classified 118 particles, achieving approximately 98% accuracy. Figure 9a shows the fitted decision boundary, and Fig. 9b–d presents the confusion matrices for the three methods, respectively." This clarification has been added in **Sect. 4.2, p. 18. in the revised manuscript.**

"Table 2 compares accuracy, precision, and recall for the three methods. Consistent with Sect. 2.3, ice crystals were the positive class for precision and recall. The metrics were calculated from the particle counts in Fig. 9 and reported as percentages rounded to whole numbers." This clarification has been added in **Sect. 4.2, p. 19. in the revised manuscript.**

Comment #12: L96: You need to cite the accuracy of conventional methods here when stating that your results are better.

Reply #12:

We thank the reviewer for this comment. The improvement reported here comes from an internal comparison on the same reference-sample test set. The shape-factor threshold method achieved approximately 94% accuracy, whereas the dual-parameter SVM method achieved approximately 98%, an increase of approximately 4 percentage points. This comparison does not establish superiority over all conventional instruments or published phase identification methods.

We have revised the Introduction and the classification-results description to state the comparison explicitly in terms of the shape-factor threshold method and the dual-parameter SVM method evaluated on the same test set. The revised wording reports the observed internal improvement without implying a general comparison with other instruments.

The corresponding text has been revised as follows: *"On the reference-sample test set, the dual-parameter SVM method achieved approximately 98% accuracy, approximately 4 percentage points higher than the shape-factor threshold method."* This clarification has been added in **Sect. 1, p. 3. in the revised manuscript.**

"On the reference-sample test set, the dual-parameter SVM method achieved approximately 98% accuracy. This was approximately 4 percentage points higher than the shape-factor threshold method and approximately 8 percentage points higher than the single-parameter DoLP method on the same test set. Combining morphological and polarization information therefore improved phase classification accuracy under the experimental conditions investigated." This clarification has been added in **Sect. 4.2, p. 20. in the revised manuscript.**

Comment #13: L105-107: Sphericity is needed as additional requirement. Non-spherical, e.g. larger droplets do change the polarization of the incident light.

Reply #13:

We thank the reviewer for this correction. We agree that optical isotropy of liquid water does not imply preservation of the incident polarization state for droplets of arbitrary shape. The polarization response also depends on scattering geometry, and nonspherical droplets may alter the polarization state.

We have explicitly restricted the droplet scattering model to approximately spherical droplets in Sect. 2.1 and revised the absolute polarization-preservation statement. The revised text distinguishes the absence of crystalline birefringence from the polarization response of scattered light. Even for a spherical droplet, differences in the amplitudes and phases of the orthogonal scattering components can change the linear polarization state under certain scattering conditions. The corresponding text has been revised as follows: *"Unlike ice crystals, liquid water can be treated as an optically isotropic medium without crystalline birefringence. The polarization scattering characteristics of approximately spherical droplets can be described by Mie scattering theory. However, the absence of birefringence does not imply that the scattered light always preserves the linear polarization state of the incident light. During scattering, the two*

orthogonal polarization components may undergo different amplitude and phase changes, producing elliptically polarized light at certain scattering angles and incident polarization orientations. This reduces the degree of linear polarization but does not necessarily reduce the total degree of polarization. For nonspherical droplets, the polarization response is also affected by particle shape and orientation. The droplet scattering model below therefore assumes approximately spherical droplets." This clarification has been added in **Sect. 2.1, p. 5. in the revised manuscript.**

Comment #14: L223-225: Please provide details on the DoFP polarization camera (polarization measurement uncertainty, resolution, name, manufacturer, etc.).

Reply #14:

We thank the reviewer for this suggestion. We have expanded the camera description in Sect. 3 and added the correction procedure and reference check in Appendix B. The instrument uses a monochrome MER2-503-36U3M POL DoFP polarization camera manufactured by DAHENG IMAGING, with a Sony IMX264MZR global-shutter polarization sensor. The native image size is 2448 × 2048 pixels, and the pixel pitch is 3.45 μm. Micropolarizers at 0°, 45°, 90°, and 135° provide four analyzer-channel measurements in a single exposure. Direct separation without interpolation gives 1224 × 1024 pixels per analyzer channel. The corresponding text has

been revised as follows: *"A monochrome division-of-focal-plane (DoFP) polarization camera (MER2-503-36U3M POL, DAHENG IMAGING) records the pattern. The camera uses a Sony IMX264MZR global-shutter polarization sensor with 2448 × 2048 pixels and a pixel pitch of 3.45 µm. As shown in Fig. 1d, micropolarizers oriented at 0°, 45°, 90°, and 135° simultaneously record four analyzer-channel intensities in a single exposure. Direct separation without interpolation produces channel images of 1224 × 1024 pixels."* This clarification has been added in **Sect. 3, p. 11. in the revised manuscript.**

Before particle measurements, dark-field correction, flat-field correction, and instrument-matrix calibration were performed. Dark images acquired at the experimental exposure and gain settings were averaged pixelwise to obtain $D_k(x,y)$. Responses measured under uniform illumination while rotating a high-extinction-ratio linear polarizer through 0°–180° were averaged for each channel and normalized by their spatial medians to obtain $F_k(x,y)$. The corrected channel intensity is given by Eq. (R2), reproduced below.

$$I_k^{\mathrm{cal}}(x,y) = \frac{I_k^{\mathrm{raw}}(x,y) - D_k(x,y)}{F_k(x,y) + \varepsilon_{\mathrm{reg}}} \qquad \text{(R2)}$$

Here, k denotes the analyzer orientation, and $\varepsilon_{\mathrm{reg}}$ is a small positive scalar regularization term. Known linearly polarized reference states were used to fit the 4 × 3 instrument matrix $\mathbf{M}$ by least squares. For a full-column-rank instrument matrix, its pseudoinverse P was then used to recover S_0, S_1, and S_2, as expressed by Eqs. (R3) and (R4), followed by DoLP calculation using Eq. (11). The complete reference-state construction and matrix-fitting procedure are provided in Appendix B.

$$\mathbf{P} = (\mathbf{M}^{\mathrm{T}}\mathbf{M})^{-1}\mathbf{M}^{\mathrm{T}} \tag{R3}$$

$$\hat{\mathbf{S}}(x, y) = \mathbf{P}\mathbf{i}^{\mathrm{cal}}(x, y) \tag{R4}$$

Figure R2, corresponding to Fig. B1 in the revised manuscript, compares the linearly polarized illumination in a particle-free region before and after correction. The mean DoLP changed from 0.969 to 1.001, reducing the absolute deviation of the mean from the expected value of 1 from 0.031 to 0.001. The estimate slightly above 1 reflects measurement and parameter-estimation errors and does not imply a physical DoLP greater than 1.

This result evaluates the correction near a fully linearly polarized reference state. The value 0.001 is a reference mean deviation, not the complete DoLP measurement uncertainty for all particles and signal conditions. Appendix B explicitly states that this check does not independently validate performance across the entire DoLP range or include all errors introduced during particle reconstruction. The corresponding text has been

revised as follows: *"Figure B1 compares the DoLP of the linearly polarized illumination in a particle-free region before and after correction. The mean DoLP values before and after correction were 0.969 and 1.001, respectively, with the corrected result closer to the expected value of 1. The corrected estimate slightly exceeds 1 because of measurement and parameter-estimation errors; this does not imply that the physical DoLP of the optical field exceeds 1. This reference check supports the correction of channel-response mismatch for states close to complete linear polarization, but it does not independently validate measurement performance over the entire DoLP range or account for all errors introduced during particle reconstruction."* This clarification has been added in **Appendix B, Fig. B1, p. 25. in the revised manuscript.**

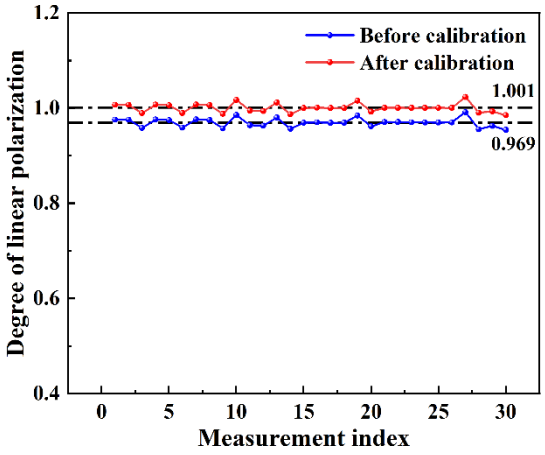

Figure R2: Degree of linear polarization of the linearly polarized illumination in a particle-free region before and after correction.

Comment #15: L322: Why 'largely' preserving and not 'preserving'. What prevents the droplets from fully preserving the polarization of the incident light?

Reply #15:

We thank the reviewer for this question. The original wording did not clearly distinguish a relatively high measured DoLP from strict preservation of the incident polarization state. The absence of crystalline birefringence does not guarantee that a droplet preserves linear polarization under all scattering conditions. Even for an approximately spherical droplet, the orthogonal scattering components can undergo different amplitude and phase changes, producing elliptical polarization at some scattering angles and incident polarization orientations. This can reduce DoLP without necessarily reducing the total degree of polarization, consistent with Eqs. (13)–(15).

The measured DoLP can also be affected by the incident polarization state, channel-response differences, noise, and reconstruction. We have revised Sect. 2.1 to explain these physical distinctions and replaced the polarization-preservation statement in the results with the observation that measured DoLP was generally higher for liquid droplets than for ice crystals under the experimental conditions investigated. This wording directly describes the reported measurements rather than assuming complete polarization preservation.

The corresponding text has been revised as follows: *"During scattering, the two orthogonal polarization components may undergo different amplitude and phase changes, producing elliptically polarized light at certain scattering angles and incident polarization orientations. This reduces the degree of linear polarization but does not necessarily reduce the total degree of polarization."* This clarification has been added in **Sect. 2.1, p. 5. in the revised manuscript.**

"Figure 8 shows the DoLP distributions of 400 particles, comprising 200 liquid droplets and 200 ice crystals. Under the experimental conditions investigated, measured DoLP was generally higher for liquid droplets than for ice crystals. Liquid droplet DoLP values were mainly distributed between 0.78 and 0.96, with an arithmetic mean of 0.857. Ice crystal DoLP values were mainly distributed between 0.66 and 0.82, with an arithmetic mean of 0.742." This clarification has been added in **Sect. 4.1, p. 18. in the revised manuscript.**

Comment #16: L409: What stands t = 0s for. Was this the injection of AgI? Why is a time frame of 10 s chosen?

Reply #16:

We thank the reviewer for this question. In Fig. 10, t = 0 s denotes the beginning of the selected observation window and does not correspond to AgI introduction. The continuous 10 s example was selected from

observations made during the later stage of the chamber experiment after AgI introduction. Its purpose is to demonstrate continuous retrieval of particle phase and microphysical parameters, including liquid droplet and ice crystal number concentrations, number fractions, LWC, and the mean equivalent diameter of the detected particles.

The 10 s duration is the interval displayed in this example, not a fixed system observation limit or the complete glaciation period beginning at AgI introduction. We have clarified the window selection, the definition of t = 0 s, and the purpose of the example in Sect. 4.3 and in the caption of Fig. 10.

The corresponding text has been revised as follows: *"To demonstrate continuous observations of cloud particle microphysical parameters, a continuous 10 s window was selected from the later stage of the chamber experiment after AgI introduction. In Fig. 10, t = 0 s denotes the start of this window, rather than AgI introduction."* This clarification has been added in **Sect. 4.3, p. 20. in the revised manuscript.**

"Figure 10: Microphysical parameter changes during a continuous 10 s window in the later stage of the ice cloud chamber experiment. The time t = 0 s denotes the start of the selected window, rather than AgI introduction." This clarification has been added in **Fig. 10 caption, p. 21. in the revised manuscript.**

~~~~~~
~~~~~~

Yours sincerely,

Prof. Dr. Xiang Xu

School of Optoelectronic Science and Intelligent Instrumentation,

Xi'an University of Technology,

Xi'an, 710048, China.

Fax: +8615529500771

Email: xxuxxiang@xaut.edu.cn